Solar Energy 196 (2020) 346–357

Contents lists available at ScienceDirect

Solar Energy

journal homepage: www.elsevier.com/locate/solener

A comprehensive review of topologies for photovoltaic I–V curve tracer

Y. Zhu*, W. Xiao

School of Electrical and Information Engineering, University of Sydney, Sydney, Australia

ARTICLE INFO

Keywords:
Photovoltaic
I–V curve tracer
Modelling
Control
Dynamics
Power converter

ABSTRACT

The I–V curve tracer is an instrument that captures the I–V characteristics of photovoltaic (PV) generators corresponding to variable environmental conditions. The device is widely used to evaluate power generation performance and detect the fault conditions of PV power generators. Various I–V tracer techniques have been developed and proposed to trace the IV characteristics and ensure high accuracy and fast speeds. A comprehensive classification and analysis was undertaken to identify the advantages and disadvantages of different technologies. This study proposes and uses five performance indices to evaluate the performance of I–V tracers. The quantitative fidelity of commercial I–V tracers were also reviewed and evaluated. This paper serves as a valuable reference tool that should be used to guide the direction of future research and lead future improvements in the field.

1. Introduction

The photovoltaic (PV) industry is experiencing fast and steady growth in terms of application, efficiency, reliability and flexibility. PV systems are expected to last a lifetime of decades. The performances of these systems need to be regularly evaluated over the long periods in which they operate. Thus, the industry requires fast and accurate ways of detecting any potential issues. Conversely, the I–V characteristics and important parameters of PV modules provided by manufacturers are based on the standard test condition (STC). The STC represents an effective testing standard; however, due to the unpredictable irradiance and temperature, the condition is rarely achievable in real-world applications. A current-voltage (I-V) curve tracer is a general term that is used to describe the ability of the technology to acquire the PV output characteristics in an efficient manner. It can be used from time to time and captures the IV characteristics of PV cells, modules, strings and arrays under a variation of solar irradiance and temperature conditions. IV characteristics are used to evaluate the generation performance of PV systems under natural sunlight in terms of power output, device degradation, and ageing effects.

One essential function in PV power systems is the maximum power point tracking (MPPT), which has been widely researched (Xiao, 2017). MPPT is an optimisation algorithm that ensures the maximum power is instantly extracted from PV sources. However, as both MPPT and I–V tracers share a common interest in relation to the maximum power point (MPP), it is sometimes difficult to distinguish between them. Notably, MPPT follows the MPP in the real-time operation of PV power systems. Conversely, I–V curve tracer is mainly used offline to detect faults and evaluate the performance of PV sources. I–V tracing captures a wide range of operating points from the open circuits to short circuits, while MPPT locks the MPP and keep the systems working at an optimal point or within a narrow range. Thus, the design and implementation of MPPT and I–V tracer differ significantly in terms of both software and hardware. It should be noted that the I–V curve tracer is not the only technology uses in PV system evaluations and fault diagnoses; however, it can be directly used. The real-time operation of fault detection and diagnosis has been used in PV power systems to detect the condition of the generators, converters, and auxiliary devices. Triki-Lahiani et al. (2018) reviewed and listed these technologies.

The acquisition of an I–V curve is important in diagnoses and evaluations of PV power generation; however, its high costs have prevents it from being widely used in the industry. Significant research has been conducted to reduce the overall costs and improve the tracking accuracy, speed and power ratings of I–V curve tracing technologies. One study summarised various methods for obtaining the I–V curve of PV modules (Duran et al., 2008). It is valuable to provide a comparison among different technologies. However, there is a strong demand for a comprehensive and in-depth analysis of different approaches in all aspects.

This paper continues the literal chronology with the latest I–V curve tracing technologies. Specifically, it classifies and compares existing I–V curve tracing technologies, power topologies and control strategies in the literature. The advantages and disadvantages of the discussed methods are summarised and compared in relation to the unified

* Corresponding author.
E-mail address: yechen.zhu@sydney.edu.au (Y. Zhu).

https://doi.org/10.1016/j.solener.2019.12.020
Received 20 May 2019; Received in revised form 18 November 2019; Accepted 6 December 2019

performance indices proposed by this study. The paper is organised as follows: First, the I–V curve and its characters are discussed. Second, five main I–V tracer typologies are classified and introduced. Third, the commercial I–V tracers are discussed and summarised. Finally, the performance indices are given for comparative study to demonstrate the effectiveness and comparison among different tracing methods.

2. The IV characteristics of PV

The I–V curve measurement is not only for research study, but it is also used in many international standards. These standards established the substantial position of the I–V curve measurement in PV system installation, commissioning and maintenance. PV characterisation and modelling are indispensable to understanding the I–V tracer. PV modelling is widely used into detect any deviations of in I–V curves. This section introduces the relevant international standards and PV modelling.

2.1. International standards

The International Electrotechnical Commission (IEC) defines many international standards for the PV energy system. The IEC 60904-1:2006 Standard describes the procedures for I–V curve measurement under different conditions and provides the measurement requirements, such as those for irradiance and temperature devices, voltage and current resolution. The IEC 60891:2009 Standard defines the I–V curve temperature and irradiance correction. The IEC 62446-1 Standard listed the documentation that must be provided to the customer. According to the requirements, the I–V curve measurement needs to be implemented in all parts of the PV system. Annex D, of the standard sets out the interpretation of a non-ideal I–V curve for PV system troubleshooting.

2.2. PV model

To verify the performance of the PV modules, a standard I–V curve is required for comparison. A PV model is used to predict the expected I–V curve shape under different conditions to compare the deviations to the measured curve. Additionally, to understand the IV characteristics of PV output, it is essential to study the mathematical model of PV cells, which are the a fundamental component of PV power systems.

A crystalline-based PV cell is constructed from a large area of silicon p-n junction, so the diode model is naturally used to represent the output characteristics of PV cells. Sabudin et al. (2017) noted that various modelling approaches represent PV output characteristics. The most common approach is based on the single-diode equivalent circuit model (SDECM), as shown in Fig. 1.

The model includes a current source in parallel with a diode. The non-ideal factors are lump summed into one shunt resistor and one series resistor. The output current from the PV cell is thus expressed as Eq. (1) and corresponds to the voltage, v_{pv} (Mahmoud et al., 2013):

$$i_{pv} = i_{ph} - i_s\left[e^{\frac{q(v_{pv}+R_s i_{pv})}{kT_c A_n}} - 1\right] - \frac{v_{pv} + R_s i_{pv}}{R_h}, \tag{1}$$

where i_{pv} and v_{pv} represent the PV cell output current and voltage respectively; R_s and R_h represent the model series resistor and shunt resistor, respectively; i_{ph} is the PV cell photon current; i_s is the diode reverse-bias saturation current; q is the charge (1.6×10^{-19} C); k is the Boltzmann constant (1.38×10^{-23} J/K); T_c is the PV cell temperature in kelvins; and A_n is the diode ideality factor.

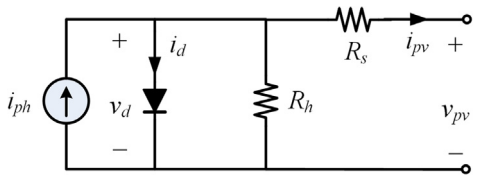

Fig. 1. Equivalent circuit of the single-diode model.

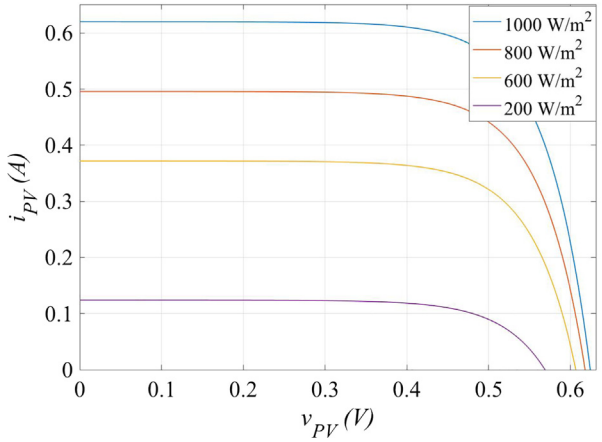

Fig. 2. Modelled I–V curve of the PV cell with constant temperature (25 °C) and variable irradiance.

The product datasheet commonly sets out the I–V curves of PV modules under STC. In relation to a new PV module, the I–V curve should be within 5% of the rated I–V curve under stable irradiance conditions. Based on the PV mathematical model, I–V curves can be simulated under different conditions. Fig. 2 and Fig. 3 illustrate the effects of changes in solar irradiance and cell temperature, respectively. It should be noted that different temperature and irradiance conditions affect the start and end points of the I–V curve. Thus, information about the open-circuit point and short-circuit point is important in the analysis of an actual PV module. The I–V curve tracer makes the measurement to the short-circuit point safer than traditional test methods.***

The I–V curve of PV output can be divided into three zones Xiao et al. (2007), as illustrated in Fig. 4 — namely, the current-source region, the power-source region, and the voltage-source region, according to the slope of the I–V curve.

2.3. I–V curve deviations

The shape of an I–V curve provides information about impairments, including damaged cells, short-circuit bypass diodes, local shading, module mismatch, increased shunt and series resistance. The IEC 62446-1 classifies the following six I–V curve shape variations for impairment signatures, as shown Fig. 5.

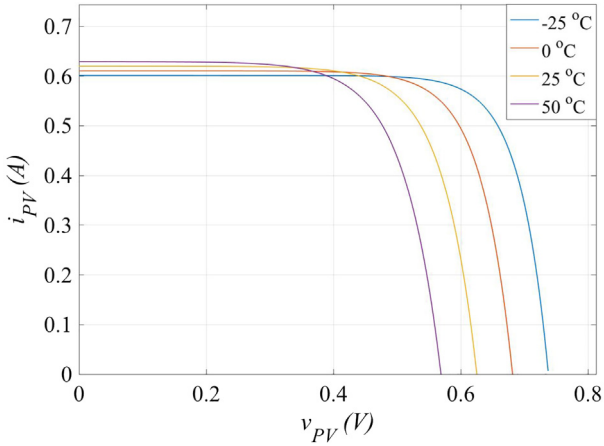

Fig. 3. Modelled I–V curve of the PV cell with constant irradiance (1000 W/m^2) and variable temperature.

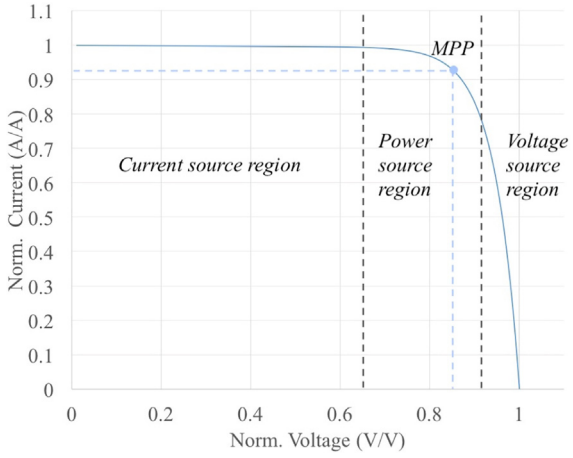

Fig. 4. Three-zone definition based on I–V curve.

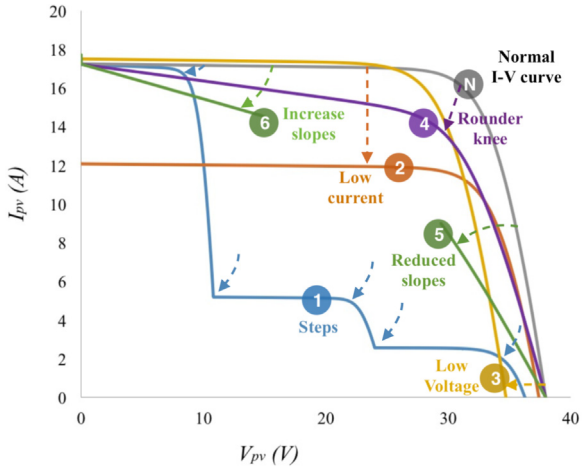

Fig. 5. I–V curve shape variation for impairment, of which the numbers 1 to 6 refers to the curve shape variations that described the standard, IEC62446.

1. Steps or notches indicate a mismatch between modules or arrays. These occur most commonly when part of the solar modules is shaded by a tree branch, building or dust, which causes the solar irradiance to be unequally distributed among the PV modules Bai et al. (2015).
2. Low current indicates uniform soiling, shading or degradation.
3. Low voltage indicates shorted bypass diodes or potential-induced degradation (PID).
4. Rounder knee indicates the ageing process.
5. A shallower slope in voltage source region indicates faults in wiring or increasing module series resistance.
6. A steeper slope in the current source region indicates shunt paths in PV cells or module mismatching.

Fault diagnosis is important if the efficiency and reliability of PV systems is to be increased. Other studies have been conducted based on I–V curve diagnostic methods can be found in Balasubramanian et al. (2013), Dhimish et al. (2017), Haque et al. (2018). The I–V curve tracer provides a fast and accurate method for verifying performance and of troubleshooting problems early.

3. Implementation topology and control strategy overview

The basic principle of I–V curve tracers is to vary PV output from the open-circuit to short-circuit condition and acquire the variation of the voltage and current. The operation includes three basic parts: data acquisition system (DAQ); power conditioner; control strategy.

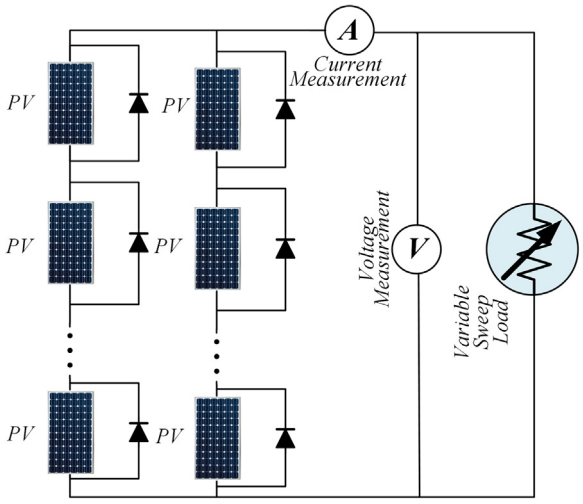

Fig. 6. Block diagram of the topology of I–V curve tracking in a PV power system.

The DAQ part of the I–V tracer is to read in the current and voltage values from the PV module terminal. The resolution of the I–V tracer depends on the number of measurement points. Commercial-scale PV arrays need to record large amounts of data; for example, the HT-Italia I–V500W can give 128 test points on each I–V curves and its internal memory can store up to 249 curves. Therefore, the DAQ of the I–V tracer needs to be fast and have large data storage spaces. The power conditioner part(e.g., the variable resistor and an electronic load) is used to change the load profile to capture the full IV characteristics of the PV source for data acquisition. The topology in this part affects the efficiency and the dynamic performance of the I–V tracer. The control strategy refers to the method used to control the power conditioner and data acquisition for the IV characteristics.

A good control strategy should accurately send the control signal to the power conditioner and effectively measure the I–V values. A typical operation of a I–V tracer is demonstrated in the Fig. 6, in which the controller senses the output voltage and current values during variable load sweeping. The methods to control the voltage value changes from zero to open-circuit voltage are based on connecting a variable load at the PV module terminals. There are five different methods to perform this task: variable resistive load method, capacitive load method, electronic load method, four-quadrant power supply method and DC–DC converter method.

3.1. Variable resistive load method

The simplest way to measure the I–V curve is to connect a variable resistor at the output terminal of the PV module. This method has been used by Amiry et al. (2018), Hammoumi et al. (2018), Rivai and Rahim (2013). The resistance value varies from zero to infinity (open circuit) to capture the points of the I–V curve from the short circuit to the open circuit.

To improve the quality of the measurement, a tracing algorithm is applied to speed up the I–V tracer. In Rivai and Rahim (2014) and Van Dyk et al. (2005), resistors combined with switches achieved smooth I–V curves. The circuit configuration is shown in Fig. 7. It uses an array of binary-numbered resistors, which connecting and disconnecting alternately, to measure the voltage and current from short-circuit to open-circuit. The switches are controlled by a micro-controller that combines the resistors to the maximum value R_{max} expressed as:

$$R_{max} = \sum_{k=0}^{n-1} 2^k R_0. \quad (2)$$

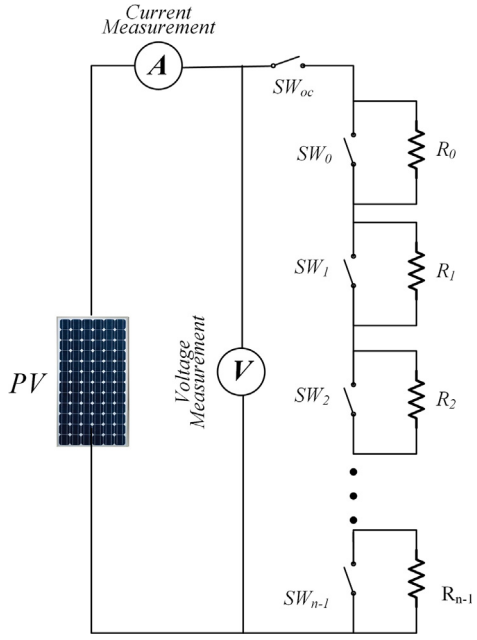

Fig. 7. Variable resistor method circuit topology proposed in Rivai and Rahim (2014).

R_0 is the smallest resistance and the resolution of the I–V curve tracer. The advantage of this method is that it can quickly produce a smooth curve (in 540.2 ms) with only eight resistors. By using this method, the resolution is fixed as the smallest resistor and the largest resistor is fixed, which makes missing measurement points close to the open-circuit voltage.

Although the variable resistive load method directly follows the principle of I–V tracing, it has a number of constraints and drawbacks. A passive resistor bank to cover the I–V tracing range is generally bulky, heavy, and difficult to adjust smoothly. It is also difficult to distribute the measurement points evenly along the I–V curve. When the resistance increases linearly, the slope of measurement points increases as a tangent function, as shown in Fig. 8. The measurement points thus become denser as they approach maximum resistance and show variable resolution. The measurement range is often limited by the range of resistors. Thus, the gap between the maximum measurement point and open-circuit voltage point can be very large. Fig. 8 shows a resistive load method using a resistor bank from 1 Ω to 400 Ω to measure the I–V curve. The blue line represents one single PV module, the red line is three of the same PV modules connecting in series, and the yellow line

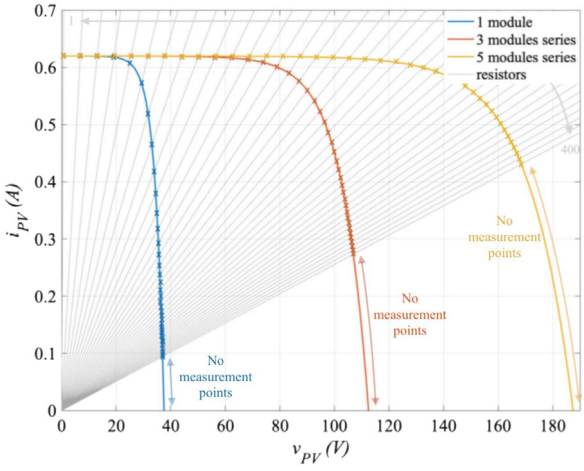

Fig. 8. I–V curve generated by variable resistor method.

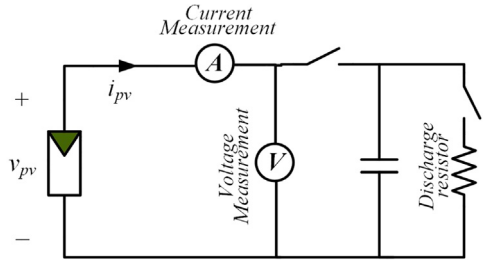

Fig. 9. Capacitive load method scheme for I–V curve tracer.

is five of the same PV modules connecting in series. The gap between the maximum measurement point and the open-circuit voltage grows as the number of modules increase. In practical situation, the irradiance and temperature also affects the I–V curve shape to make this method inflexible to cover the entire voltage source region with good resolution. Furthermore, the PV energy cannot be recycled during the test period.

3.2. Capacitive load method

The capacitive load method involves using capacitors for I–V tracer applications. As the charge of the capacitor increases, the current drops and the voltage rises. This charging process allows the I–V curve to be obtained passively. The measuring circuit commonly used in this method is shown in Fig. 9. The basic circuit and hardware prototype can be found in Aguilar et al. (2017) and Recart et al. (2006a). The voltage and current are measured directly from the terminal of the PV module. The resistor connected with the switch is used to discharge the power after a test.

The capacitor bank can be sized to accommodate the measurement time and the required resolution. Research focuses on advanced feature to improve the tracking performance (Spertino et al., 2015; Mahmoud, 2006). The capacitor array can also be associated with active switches to fit different ranges of the I–V tracking requirement (Xiong et al., 2018). It has been reported that the capacitive load method can trace the PV array with an open-circuit voltage of up to 500 V and a short-circuit current of up to 20 A (Chen et al., 2018). Furthermore, research proves the fast speed of the proposed method, Spertino et al. (2013), which can sweep the whole I–V curve within 500 ms in a 62 W PV module. Additionally, Bifaretti et al. (2012) and Spertino et al. (2016) used capacitive load method to find the global MPP. The capacitive load method is commonly used for commercial portable I–V tracers, such as the Solmetric PVA1000.

The principle of the capacitive load method is simple and the measurement time can be short. However, the method requires a significant volume of capacitance, especially for large-scale PV arrays. Fig. 10 gives the capacitance for I–V tracing calculated using 65 different PV modules and different PV array connections of popular PV panel manufacturers (e.g. LG Energy, SunPower, REC, Winaico, and Q Cells). To measure the different I–V curves, the tracing capacitors need to cover a large range of capacitance, voltage, and inrush current. Consequently, the physical size and the costs of the capacitor are high. Additionally, the testing time is highly dependent upon the PV parameters and capacitors charging behavior. Further, the bandwidth requirement for DAQ is critical to cover the non-linear I–V curve accurately. According to Spertino et al. (2015), fidelity can deviate from the true I–V curve with a measurement uncertainty of ± 1%.

3.3. Electronic load method

The electronic load method uses a transistor as the load. The transistors are usually a metal oxide semiconductor field effect transistor (MOSFET), a bipolar junction transistor (BJT) or a insulated-gate bipolar transistor (IGBT) (Batista et al., 2012; Leite and Chenlo, 2010;

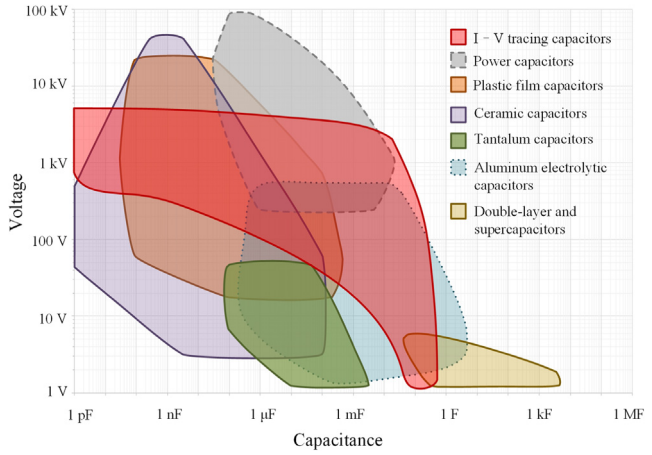

Fig. 10. I–V tracing capacitor capacitance and voltage range among all different type capacitors.

Sahbel et al., 2013). The voltage between the drain to the source is modulated via the gate source voltage (MOSFET and IGBT) or current (BJT). Therefore, the circuit can quickly scan the IV characteristics of the PV modules.

The MOSFET (the most common electronic load) changes the gate-source voltage (V_{GS}) to control the drain current (I_D). The basic circuit utilised for this method is shown in Fig. 11, where I_{PV} and V_{PV} are the output current and voltage of the PV module, and V_{DS} is the drain source voltage.

Together, the I–V curves of the MOSFET and PV module illustrate the matching point when the gate signal, V_{GS}, is accordingly varied (Fig. 12). The drain current I_D and PV output current I_{PV} are the same; thus, the measuring points are the equality points in Fig. 12.

The characteristic of a MOSFET as follows.

For the triode region:

$$I_D = K_N(2(V_{GS} - V_{th})V_{DS} - V_{DS}^2), \tag{3}$$

For the saturation region:

$$I_D = K_N(V_{GS} - V_{th})^2, \tag{4}$$

where K_N is the device constant, V_{th} is the threshold voltage.

The measuring points comprise the intersection of the I–V curve of the PV module and the $I_D - V_{DS}$ curves of the MOSFET. The equation for the intersection points can be written as:

$$I_D = I_{pv}. \tag{5}$$

By changing the V_{GS} in a suitable range, the measuring points can sweep between I_{SC} and V_{OC}.

The innovation of this method is that the measurement is according to current ramp instead of voltage ramp. As far as the PV module is concerned, the MOSFET method can provides linear changing measurement points in the voltage source region, where I_D changes approximately linearly with V_{GS}. However, for V_{pv} in the power region and

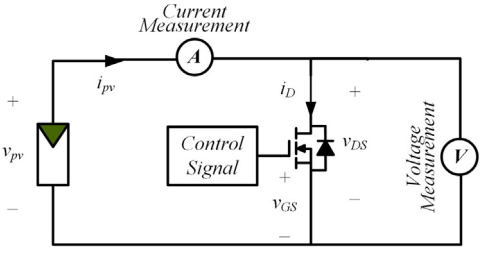

Fig. 11. Basic schematic circuit for I–V curve tracer using MOSFET as electronic load.

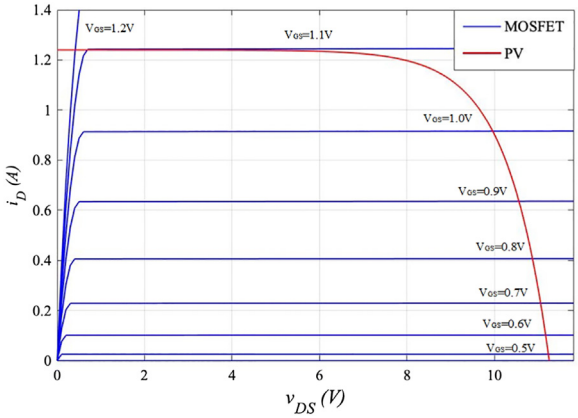

Fig. 12. A comparison of the I–V characteristics of MOSFET and the PV module output.

current-source region, the I–V curve is nearly flat, making V_{pv} is sensitive to a small variation of V_{GS}. The measuring points move quickly in the power region and the current-source region. This limitation can be improved by introducing control circuits, such as a DC–DC converter.

There are two approaches to control for scanning the I–V curve with evenly operation points. The first approach applies a low-frequency scan signal to control and vary the gate voltage of the MOSFET in order to track the complete range of PV module characteristics. The scan signal can be a sine wave Kuai and Yuvarajan (2006) or a coded signal from a micro-controller (Willoughby and Osinowo, 2018; Papageorgas et al., 2015). The second approach is to use a DC–DC converter to control the gate-to-source voltage of the MOSFET, V_{GS}. Leite et al. (2014) designed and used the PWM to control a buck-boost converter and output controllable voltage for I–V curve tracing. The signal from the converter output corresponding to the V_{GS} can produce a proportional I_D, which sweeps from zero to short-circuit current. Although the control approaches can overcome the limitation of the MOSFET I–V tracer measurement in the current-source region and power region, the resolution is less sufficient compared with other methods.

The MOSFETs can be paralleled to reach a higher output current to measure PV strings or arrays. However, the maximum rating of a linear MOSFETs is 1000 V and 520 W Kuai and Yuvarajan (2006). The cost of high-quality power MOSFETs are high. Thus, the I–V curve tracer is not efficient for high PV output measurements.

The topology for using the BJT as an electronic load is based on a principle of transistor operation mode similar to the MOSFET topology. As the base current I_B increases, the collector current I_C in turn increases and the voltage V_{CE} decreases (Recart et al., 2006b). Hence, the transistor acts as a variable resistor at the terminal of the PV panel. To control I_B, a microcontroller or a function generator can be used to provide a ramp or a sinusoid wave current signal to the base of BJT. The change in the operating point during the preceding method is fast. Henni et al. (2017) added a capacitor to slow down the I_B change. As state above, this method is based on BJT configuration; thus, its application limit on PV cell level (Guvench et al., 2004) or single-panel level (Henni et al., 2017).

The IGBT topology operation principle is the same as that of the MOSFET topology. Leite et al. (2014) used an IGBT and two series capacitors to monitor the characteristics of high voltage PV strings. It should be noted that for the MOSFET and the IGBT, the control signal is a voltage signal, which is easier to generate. Further, the MOSFET and the IGBT load have a higher maximum rating and faster sweeping speed.

The drawback of this method is that all the power is consumed by the transistor, which can cause the device temperature to exceed its tolerance. A heatsink can be used to help release the heat; however, this makes the device bulky and heavy. Even mounted on a heat sink, the

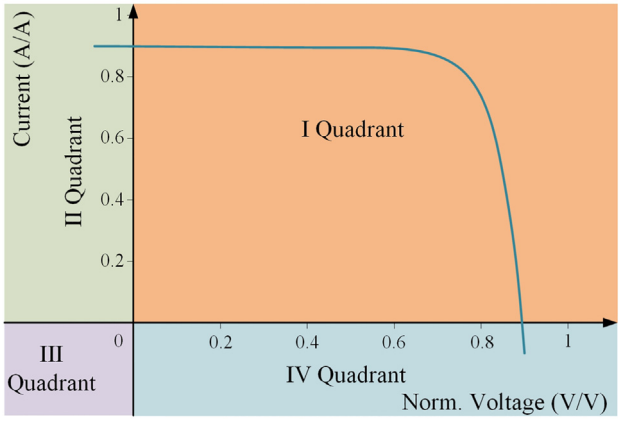

Fig. 13. An I–V curve taken with a four-quadrant power supply.

robustness of the circuit with high-power PV strings cannot stand such power in the active region for a long period Asghar (2004).

3.4. Four-quadrant power supply method

Some researchers use a four-quadrant power supply to test the IV characteristics. The four-quadrant power supply is the equipment that supplies and dissipates power. It is usually used to simulate the DC power supply, load, PV arrays and batteries. The system can operate in four quadrants (Fig. 13). The PV modules are designed to be used in the first quadrant. However, the points around the axes are an important diagnosis indicator of mismatching effects (Hecktheuer et al., 2002).

The topology of this method is simple—the PV module directly connects to a four-quadrant power supply that is controlled by a computer, as shown in Fig. 14. The voltage and current values are read and stored as the sweep is performed.

In previously proposed systems, different methods were developed to control voltage. Voltage sweeping can be controlled manually (Malik and Damit, 2003) or by generating a voltage ramp (Fernández-Reche et al., 2006; De Blas et al., 2002). Piliougine et al. (2011) developed a new measuring procedure using two voltage ramps to capture more points at the knee part of the I–V curve. This measure improved the measurement accuracy of the MPP and open-circuit point.

The four-quadrant power supply method is the fastest and most accurate of the four methods. A control strategy can easily be added by directly programming a computer. The measurement rating can reach to 1000 V/100 A. However, the four-quadrant power supply is costly and bulky. Consequently, this method has been limited to laboratory experiments.

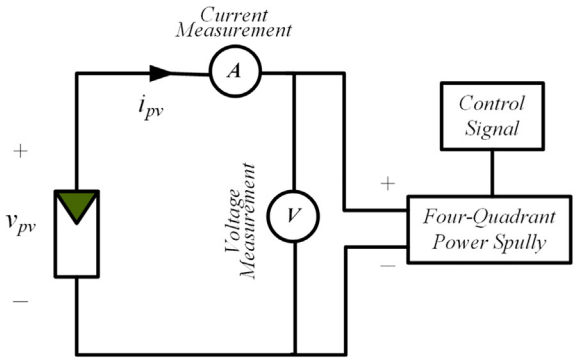

Fig. 14. Basic schematic circuit for I–V curve tracing using four-quadrant power supply method.

3.5. DC–DC converter method

The voltage conversion ratio of DC–DC converters can be used to vary virtual resistance at the input terminal and serve as the I–V tracer. Fig. 15 shows the commonly used DC–DC converter topologies including buck-boost, Cuk, Zeta and single-ended primary-inductor converter (SEPIC). The converter and load can be programmed to flexibly emulate a resistive load, a controllable current load, or a controllable voltage load. The DAQ system cooperates with the programmable DC load to provide a more accurate measurement. Additionally, the DC–DC converter method is highly efficient and low in costs. However, one drawback of the DC–DC converter method is that power switching causes a ripple of voltage and current.

Previous research focused on the optimal utilization of DC–DC converters for I–V curve tracing (Tse et al., 2004; Durán et al., 2012). The switching-mode converters should deal with the measurement ranges in continuous conduction mode (CCM) and discontinuous conduction mode (DCM), switching ripples and component efficiency. Thus, the dimensionless parameter, K, is used to measure the conduction mode. K is given by:

$$K = \frac{2L_{eq}f_s}{R}. \tag{6}$$

when K is larger than critical value K_{crit}, the converter operates in CCM; when K is smaller than K_{crit}, the converter operates in DCM. The relationships between the emulated resistance at the output (R_i), equivalent inductance (L_{eq}), duty cycle (D) and the real load connected on the converter (R) are summarised in Table 1 Durán et al. (2009).

Among the basic DC–DC converter topologies, buck converter cannot emulate small impedances to measure values near the short-circuit current of the I–V curve; boost converter cannot emulate large impedances to measure the values near the open-circuit voltage of the I–V curve. Therefore, buck converters and boost converters with resistance load topologies are not suitable for I–V curve tracing applications (Tse et al., 2004; Durán et al., 2009).

From above, the buck-boost derived converter is the only configuration to sweep the whole I–V curve of a PV module in CCM. The topologies that provide the same conversion ratio include buck-boost, Cuk, SEPIC and Zeta. A comparative study with the goal of choosing a suitable converter topology for the application of the DC–DC I–V tracer is provided in the following section.

To ensure a fair comparison, all the converters were physically designed for the same PV module with the same current and voltage ripple, listed in Table 2. The parameters are defined in the table and referred to the PV model in Fig. 1. The peak-to-peak values of the indicator current ripple and capacitor voltage ripple are assigned the same for the four different converter topologies. The parameters of the indicator and the capacitor can be determined and based on the MPP condition of the PV module. The values of the passive components for the converters are tabulated in Table 3. Furthermore, the RMS current values for important components are computed in Table 4 to determine the operating conditions and conduction loss of each element in the circuit. The variable used in the tables refers to the definition in converter circuits, as shown in Fig. 15.

When considering the inductor in the topologies, neither shows advantages over the other. Buck-boost topology only requires one input inductor to achieve the same ripple of inductor current. However, its RMS current through the inductor is the largest of the four topologies. In relation to the Cuk, SEPIC and Zeta topologies, two inductors split the current ripple equally; thus, the RMS values on inductors were lower than buck-boost topology (Dian et al., 2014).

In considering the input capacitors (C_{in}), Cuk and SEPIC topologies require the smallest capacitance and RMS current value (Babaei and Mahmoodieh, 2014; Safari and Mekhilef, 2011). A small and cheap capacitor can fulfil this requirement. The input capacitors in buck-boost and Zeta topologies are required to supply the energy to the load when

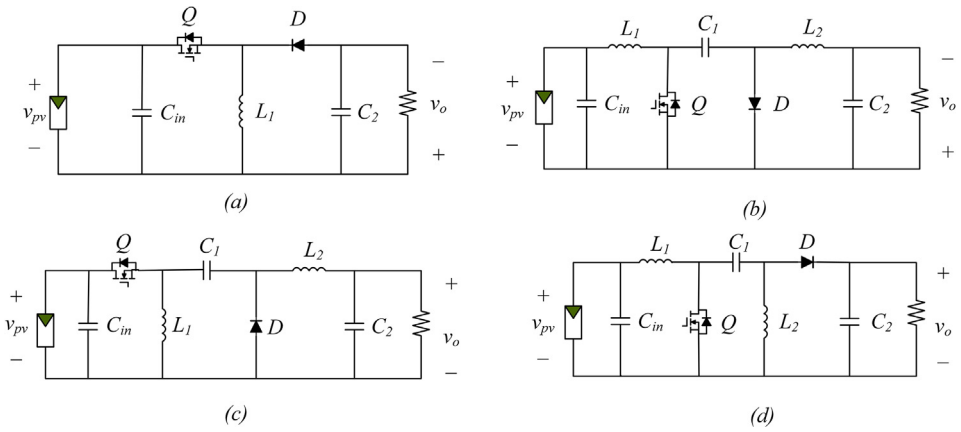

Fig. 15. Commonly used DC–DC converters in PV side power interface: (a) Buck-boost converter. (b) Cuk converter. (c) Zeta converter. (d) SEPIC.

energy is increasing in the inductor, and a large capacitor is needed to smooth the discontinuous current. As the output current in Cuk and Zeta topologies is continuous, a small output capacitor (C_2) is sufficient to smooth the voltage. The output capacitors in buck-boost and SEPIC topologies provide the load current when energy is decreasing in the inductor. Thus, the output capacitor must have enough capacitance to meet the requirement for the output voltage ripple. The coupling capacitor that indicated as C_1 is required by the converters of Zeta, Cuk and SEPIC. The study showed that the current stress of C_1 is the same for the three different topologies. Therefore, there was no difference in conduction loss among the converters.

The selection of the power MOSFET (Q) should handle the peak voltage and currents while minimising power dissipation losses. The maximum voltage for all topologies are the same, which is $V_{IN(max)} + V_{OUT}$, and the peak-current rating is also the same for all the topologies as $I_Q = I_{IN} + I_{OUT} + \Delta I_L$. The power dissipation losses are related to RMS current values. SEPIC and Zeta topologies have a lower current rating than another two topologies (Riley, 2014). The diode selection is similar to the switch selection, and SEPIC and Zeta topologies show more advantages than buck-boost and Cuk topologies.

Table 5 summarises the properties of each topology. It should be note that buck-boost topology is the worst performing topology, and requires significant components to smooth the input and output currents.

It is necessary to conduct a dynamic analysis of the converter topologies to find a fast and stable method to sweep whole I–V curve (Xiao et al., 2007; Zhu, 2018). In the following section, the modelling analysis is demonstrated using buck-boost, Cuk, SEPIC and Zeta topologies. The symbols used in this section are the same as previous (Table 2). The system dynamics can be expressed in a general form of the inductor current (i_L) and PV voltage (v_{pv}) which is controlled by the switching duty cycle (d).

Table 2
PV model parameters for comparison.

Symbols	Definition	Value
$\mathbf{E_{STC}}$	Irradiance at STC*	1000 W/m^2
k	Boltzmann constant	1.38×10^{-23} J/K
q	Charge	1.6×10^{-19} C
$\mathbf{T_{CS}}$	PV cell temperature at STC	298 K
$\mathbf{V_{TCS}}$	Thermal voltage of p-n junction at STC	25.7 mV
$\alpha_\mathbf{T}$	Temperature coefficient on PV current(%/°C)	− 0.36
$\beta_\mathbf{T}$	Temperature coefficient on PV voltage(%/°C)	− 0.36
$\mathbf{A_n}$	Diode ideality factor	2.0811
$\mathbf{R_s}$	Series resistance	0 Ω
$\mathbf{R_h}$	Shunt resistance	4.6433×10^{-3} Ω
$\mathbf{N_s}$	Number of cells in series	36
$\mathbf{N_p}$	Number of cells in parallel	1
$\mathbf{V_{OCS}}$	PV open-circuit voltage at the STC	22.5 V
$\mathbf{I_{SCS}}$	PV short-circuit current at the STC	0.62 A
$\mathbf{I_{MS}}$	PV current at the maximum power point (MPP) at the STC	0.56 A
$\mathbf{V_{MS}}$	PV voltage at the maximum power point (MPP) at the STC	18.00 V
f_s	Switching frequency	40 kHz
I	Maximum inductor current ripple	15%
V	Maximum input voltage ripple	5%

$$\frac{di_L}{dt} = f\left(i_L, v_{pv}, d\right), \tag{7}$$

$$\frac{dv_{pv}}{dt} = g\left(i_L, v_{pv}, d\right). \tag{8}$$

The small-signal model can be further derived by:

$$\frac{d\tilde{i}_L}{dt} = \frac{\partial f}{\partial v_{pv}}\tilde{v}_{pv} + \frac{\partial f}{\partial i_L}\tilde{i}_L + \frac{\partial f}{\partial d}\tilde{d}, \tag{9}$$

Table 1
Relationship of R_i and K for common DC–DC converters.

Converter	K_{crit}	R_i (CCM)	R_i range (CCM)	R_i(DCM)	R_i range (DCM)
Buck	$1 - D$	$\frac{R}{D^2}$	$[R, \infty)$	$\frac{R}{4}\left(1 + \sqrt{1 + \frac{4K}{D^2}}\right)^2$	$\left[\frac{R}{4}(1 + \sqrt{1 + 4K})^2, \infty\right)$
Boost	$D(1 - D)^2$	$R(1 - D)^2$	$[0, R)$	$\frac{4R}{\left(1 + \sqrt{1 + \frac{4D^2}{K}}\right)^2}$	$[4R/(1 + \sqrt{1 + 4/K})^2, R)$
Buck-boost derived	$(1 - D)^2$	$\frac{R(1-D)^2}{D^2}$	$[0, \infty)$	$\frac{KR}{D^2}$	$[KR, \infty)$

With $K = \frac{2L_{eq}f_s}{R}$ and $\frac{1}{L_{eq}} = \frac{1}{L_1} + \frac{1}{L_2}$; DCM occurs when $K < K_{crit}$.

Table 3
Circuit parameters of different Converter Topologies.

Topology	Inductance	Capacitance
Buck-Boost	$L_1 = 2.1 \times 10^{-3}\ H$	$C_{in} = 9.33 \times 10^{-6}\ F\ C_2 = 1.33 \times 10^{-5}\ F$
Cuk	$L_1 = 2.1 \times 10^{-3}\ H\ L_2 = 2.1 \times 10^{-3}\ H$	$C_1 = 1.33 \times 10^{-5}\ F\ C_2 = 2.92 \times 10^{-7}\ F$
SEPIC	$L_1 = 2.1 \times 10^{-3}\ H\ L_2 = 2.1 \times 10^{-3}\ H$	$C_1 = 1.33 \times 10^{-5}\ F\ C_2 = 1.33 \times 10^{-5}\ F$
Zeta	$L_1 = 2.1 \times 10^{-3}\ H\ L_2 = 2.1 \times 10^{-3}\ H$	$C_1 = 1.33 \times 10^{-5}\ F\ C_2 = 2.92 \times 10^{-7}\ F$

Table 4
RMS current Values of converter components.

Components	Buck-boost	Cuk	SEPIC	Zeta
C_{in}	1.0089	0.0242	0.0242	0.8747
C_1		0.8745	0.8745	0.8745
C_2	0.9800	0.0242	0.8750	0.0242
MOSFET	1.2650	1.1135	0.4059	0.4059
Diode	1.5493	1.3638	0.4972	0.4972
L_1	2.0001	0.5605	0.5605	0.5605
L_2		1.2002	1.2002	1.2002

$$\frac{d\widetilde{v}_{pv}}{dt} = \frac{\partial g}{\partial v_{pv}}\widetilde{v}_{pv} + \frac{\partial g}{\partial i_L}\widetilde{i}_L + \frac{\partial g}{\partial d}\widetilde{d}. \tag{10}$$

A dynamic resistance (R_{pv}) is used to represent the nonlinear relationship of PV output voltage and current in the dynamic model. It is given by:

$$R_{pv} = \frac{\widetilde{v}_{pv}}{\widetilde{i}_{pv}}. \tag{11}$$

Fig. 16 shows the value of the dynamic conductance (G_{pv}) and resistance (R_{pv}) change with the operating point in the I–V curve. The resistance rises quickly when the operating point approaches to the MPP. In the regions' open circuit voltages, the dynamic resistance is invariant.

Each time duty ratio changes, the voltage and current value has a small period of fluctuation, which affects the accuracy of the current measurement. To eliminate the effects of this disturbance, the measurement should wait longer than the settling time when the dynamic response settles to a steady state. A system's settling times can be calculated with the undamping nature frequency and damping ratio. The settling time for each topology of all operation points on the I–V curve is illustrated in Fig. 17.

For all topologies, the systems take the longest time to settle down in the short-circuit point. The settling time is 8.447 s for buck-boost and Zeta topologies, and 0.264 s for Cuk and SEPIC topologies. The settling time decreases when the voltage increases for all topologies. In the voltage source region, the settling time has little variation and approaches to zero. In open-circuit voltage point, the settling time is 8.920×10^{-6} s for Cuk and SEPIC topologies, and 2.855×10^{-4} s for buck-boost and Zeta topologies. The Cuk and SEPIC topologies can reach to steady-state a hundred times faster than buck-boost topology. By dynamic comparison, the Cuk and SEPIC topologies demonstrate better dynamic characteristics than the other two topologies. Table 6 summarises both the component efficiency and dynamic performance for each topology.

Some tracing algorithms are applied to the DC–DC converter

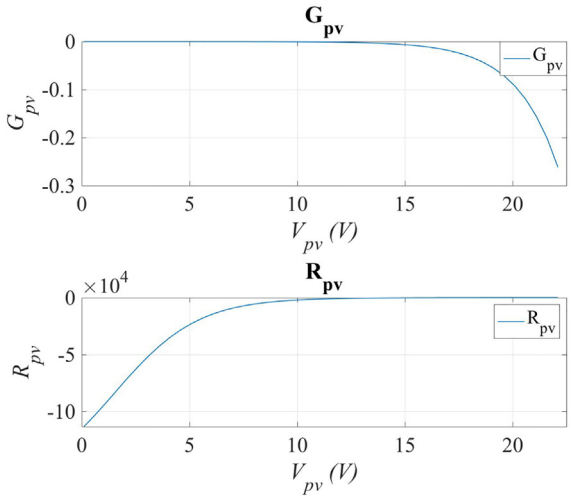

Fig. 16. IV characteristics of the PV module of dynamic conductance and resistance.

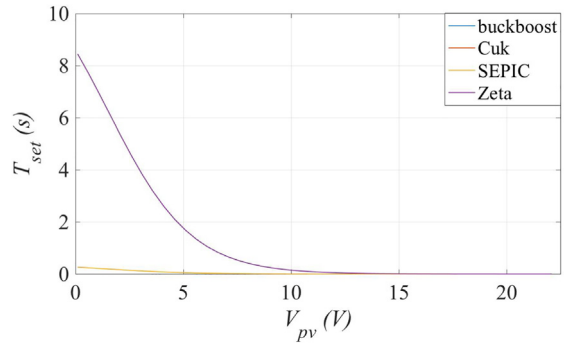

Fig. 17. Comparison of system settling time of buck-boost, Cuk, SEPIC and Zeta topologies.

method to improve the quality of the I–V curve. Spiliotis et al. (2017) used a voltage and current sweep combined tracing algorithm to achieve good resolution. In the flat region near I_{SC}, the method uses voltage sweeping. Between V_{OC} to 92–95% of I_{SC}, the method uses current to sweep. The method uses the local MPP as the division of two modes. This method offers a significant improvement in accuracy and a major reduction in measurement efforts.

An adaptive I–V curve detecting method is introduced in Zhu (2018). This new algorithm uses the current increment to decide the change of the duty factor. When the current increment is low in value

Table 5
Components characteristics of different topologies.

Converter topology	Inductor	Input Capacitor	Output Capacitor	Power MOSFET
Buck-boost	High RMS current	High capacitance	High capacitance	High current rating
Cuk	Need two inductors, Low RMS current	Low capacitance	Low capacitance	High current rating
SEPIC	Need two inductors, Low RMS current	Low capacitance	High capacitance	Low current rating
Zeta	Need two inductors, Low RMS current	High capacitance	Low capacitance	Low current rating

Table 6
Component efficiency and dynamic performance of different topologies.

Topology	Component efficiency	Dynamic performance
Buck-boost	Very low efficiency	Slow dynamic performing
Cuk	High efficiency. Need expensive MOSFET to handle high current rating.	Fast dynamic performing
SEPIC	High efficiency. Need large capacitor in output to smooth output voltage	Fast dynamic performing
Zeta	High efficiency. Need large capacitor to smooth input current.	Slow dynamic performing

Table 7
General comparison between the different types of tracing methods.

Tracing method	Accuracy	Sweep speed	Maximum rating	Resolution
Resistive load	Low	Low	Low	Low
Capacitive load	Medium	Medium	High	Medium
Electronic load	Medium	Medium	Low	Medium
Four-quadrant power supply	High	High	Low	High
DC–DC converter	High	Medium	High	High

(i.e., the I–V curve has only a few changes), the incremental step of switching duty cycle increases, making the next measurement further from the previous operation point. In addition, this method also has a time tuning parameter to adjust the dynamic behaviour of the electronic load.

Table 7 summarises the properties of each method and compares all of the factors. The performance of each method is gauged qualitatively in terms of Low, Medium and High.

4. Review of commercial products

The current market has developed many I–V tracers since 2011. Different companies have developed different products to meet their specific aims. This has led to many differences in the properties of I–V tracers. In this section, commercial I–V tracers are reviewed and compared in relation to four properties: sweep speed, range and resolution, data analysis and troubleshooting, and size.

4.1. Sweep speed

Sweep speed refers to the time required for an I–V tracer to complete one sweep of the measure from short-circuit to open-circuit. A fast sweep speed is essential to an I–V tracer, as it ensures that all points on the curve are obtained under the same condition. Current I–V tracers on the market have the sweep time between 2 s to 300 s. The most portable I–V tracers use the capacitive load method. Sweep speed depends on the capacitor charging time. For string-level measurement, the charging time can be up to 10s. Sweep speed can also be limited by the sensor speed and micro-controller read-in speed. In relation to the DC–DC converter load method, the sweep speed is limited by the ripple settling time. To achieve a good dynamic performance, settling time can be up to 8 s for one measurement point. Thus, the circuit design and control algorithm are important for the DC–DC converter load method,as they reduce the sweep time.

4.2. Range and resolution

I–V curve tracers are limited by the voltage and current measurement ranges. Absolute resolution refers to the smallest change that the I–V tracer can detect. The EKO tracer (model MP-180) has the highest resolution in the market(2.4 μV). It should be noted that the absolute resolution corresponds to the range of PV voltage and current. A PV string voltage can reach to 1000 V. In relation to PV cell development and evaluation, the voltage range is generally lower than 20 V. I–V tracing should also focus on the resolution near the region of the MPP, which should be accurately acquired to represent the maximum power output.

4.3. Data analysis and troubleshooting

Based on extensive field experience, many companies have developed their troubleshooting functions. Following I–V curve measurement, some devices offer troubleshooting assistance. For example, Solmetric provides a flowchart for troubleshooting, that includes verifying that the test returns a useful I–V curve, identifying the normal shape and detecting the deviation Hernday (2014).

4.4. Size

In commercial PV systems, I–V curve tracers are generally measured in combiner boxes during a regularly scheduled site maintenance. However, technicians have to measure each panel when troubleshooting. I–V tracers need to be small in size so that they are easy to carry. Popular products, such as I–V500w(HT Italia) and SOLAR-600 (Amprobe), are both small in size and are lightweight.

A brief review of commercial I–V tracers is summarised in Table 8. The weights and prices shown in the table are based on kilograms and US dollars. The Daystar, Kewell, Qunling and Solmetric I–V tracers use the capacitive load method. The EKO I–V tracer uses the DC–DC converter method.The other three methods have not been used in industrial applications. The capacitive load method has a well-established role in the industrial field; however, when measuring high voltage PV strings, it takes an extremely long time to charge. The measurement range and resolution progress are limited by the component properties. The DC–DC converter method could represent a future trend in I–V tracers,

Table 8
Comparison of commercial I–V tracers.

Company	Product	Sweep speed	Range	Resolution	Weight	Data analysis	Price in 2019
HT-Italia	I-V500w (2015-05-17)	5 s	1500 V, 15 A	0.1 V, 0.01 A	1.2 kg	yes	$4495.00
Solmetric	PVA-1000S (2014-02)	0.05–2 s	1000 V, 20 A	25 mV, 2 mA	5.44 kg	yes	$5695.00
Amprobe	SOLAR-600 (2010)	3 s	60 V, 12 A	10 mV, 10 mA	1.16 kg	no	$2299.95
EKO	MP-180 (2016)	0.005–300 s	20 V, 20 A	0.24–2.4 μV, 0.24 A	9 kg	yes	$2244.00
Daystar	DS-1000 (2016-01)	0–10 s	1000 V, 100 A	0.4 V, 50 mA	14.4 kg	no	–
PVE	PVPM1500X (2018-06-01)	0.02–2 s	1500 V, 20 A	0.01–0.25 V, 0.005–0.01 A	8.5 kg	no	–
Kewell	IVT-200-1000 (2017-09)	10 s	1000 V, 20 A	0.1 V, 0.01 A	n/a	no	$1455.00
Qunling	PV-8150K (2013-01)	15 s	1000 V, 200 A	1 V, 0.1 A	10 kg	yes	–
Seaward	PV210 (2017-09-03)	–	1000 V, 15 A	0.1 V, 0.01 A	1.04 kg	no	$2595.00

as the control algorithm can be added to the method to obtain more stable and accurate measurements. To meet market expectations, more progress is required to reduce sizes and decrease prices.

5. Performance indices

Performance indices are used to qualify the health of the PV modules and as I–V tracer performance metrics. As I–V tracer fidelity is difficult to evaluate, the performance indices can help assess the accuracy for topology comparisons. The indices can be categorised into performance factor, deviation on critical points and full curve, fill factor, voltage ratio and current ratio, and slope deviation. These five indices can be used to estimate different I–V tracer measurement properties that are independent but interrelated.

5.1. Performance factor

The performance factor is used to assess the deviation between the PV model and measurement values, as expressed in Eq. (12). If the measured and predicted P_{max} are in accord, the performance factor is 100%. A high quality I–V tracer should have performance factor value close to 100% when measuring a newly constructed array.

$$Performance\ factor = \frac{P_{max}(measured)}{P_{max}(predicted)}, \tag{12}$$

where P_{max} represents the maximum power.

5.2. Deviation on critical points and full curve

The deviation on critical points includes the open-circuit point and short-circuit point. The open-circuit voltage and short-circuit current deviation indices D_{OC} and D_{SC} indicate how accurately the I–V tracer output represents the terminals of the I–V curve (Huang et al., 2016):

$$D_{OC} = \sqrt{\left(\frac{\widetilde{V}_{OC}}{V_{OC}} - 1\right)^2}, \tag{13}$$

where $\widetilde{V}_{OC}$ and V_{OC} represent the open-circuit voltage values from the I–V tracer measurement and the product datasheet, respectively.

$$D_{SC} = \sqrt{\left(\frac{\widetilde{I}_{SC}}{I_{SC}} - 1\right)^2}, \tag{14}$$

where $\widetilde{I}_{SC}$ and I_{SC} represent the short-circuit current values from the I–V tracer measurement and the product datasheet, respectively.

The indices on critical points measure the accuracy of the I–V tracer from the product datasheet. However, the full I–V curve performance cannot be evaluated. Mahmoud et al. (2013) defined a full I–V curve performance indicator for a simulation model and real system. The same indicator can be used to estimate the performance of I–V tracer. The deviation of the PV current between the I–V tracer measurement and product datasheet can be calculated by the root-mean-square deviation (RMSD) using voltage as a reference and can be expressed as follows:

$$\mathrm{RMSD}(I) = \sqrt{\frac{\sum_{j=1}^{N}(\widetilde{I}_j - I_j)^2}{N}}, \tag{15}$$

where $\widetilde{I}_j$ represents the current from the I–V tracer and I_j represents the current from the datasheet.

Mahmoud et al. (2013) also recommended the use of a normalized RMSD (NRMSD) to uniform the performance indicator for different sizes and materials of PV cells. The NRMSD is expressed as

$$NRMSD = \frac{\mathrm{RMSD}}{I_{sc}}. \tag{16}$$

5.3. Fill factor

Fill factor is an indicator of the squareness of the I–V curve; it is expressed as in Eq. (17):

$$Fill\ factor = \frac{I_{mpp} \times V_{mpp}}{I_{SC} \times V_{OC}}, \tag{17}$$

where I_{mpp} and V_{mpp} represent the MPP current and voltage values, respectively.

The ideal PV cell has a rectangular-shaped I–V curve of FF = 1. A squarer curve indicates a higher output power and higher module efficiency. Modules should have similar fill factors of given manufactory parameters under similar environmental conditions. If the fill factor differs from the manufactory parameters, the voltage ratio and current ratio need to be tested to identify the problem.

5.4. Voltage ratio and current ratio

The voltage ratio and current ratio are embedded in the fill factor equation. The ratio values are an approximation of the slopes of the horizontal and vertical parts of the I–V curve. The voltage ratio and current ratio are expressed in Eqs. (18) and (19).

$$Voltage\ ratio = \frac{V_{mpp}}{V_{OC}}, \tag{18}$$

$$Current\ ratio = \frac{I_{mpp}}{I_{SC}}. \tag{19}$$

Inaccurate data can be caused by irradiance or temperature changes significantly during the measurement. To avoid this, the I–V curve tracer needs to be able to capture the full curve data in 1 s.

5.5. Slope deviation

In relation to the aforementioned methods, the measurement points are not evenly located on the I–V curve. Thus, an additional performance indicator should be calculated to define the efficiency of the measurement point distribution. The indicator uses the PV model as a reference. The difference between the current measure point slope (k), the slope of the previous measure point ($k1$) and following measure point ($k2$) calculated by the root-mean-square deviation, shown in Fig. 18. The slope deviation is mathematically expressed as

$$\mathrm{RMSD}(k) = \sqrt{\frac{\sum_{i=1}^{N}(k_{1i} - k_i)^2 + \sum_{i=1}^{N}(k_{2i} - k_i)^2}{N}}. \tag{20}$$

If the RMSD(k) equals zero, the measurement curve is an ideal a smooth curve.

6. Conclusion

The paper comprehensively reviewed and analyzed the technology

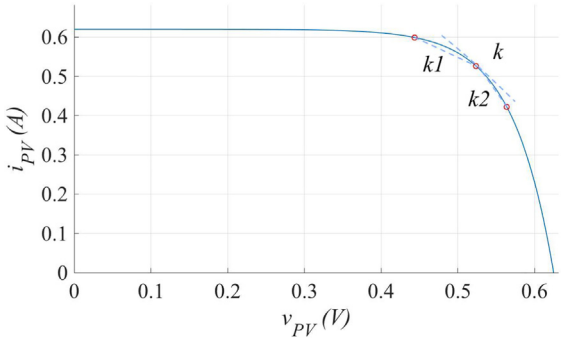

Fig. 18. Graphical representation of the RMSD (k).

of I–V curve tracers. The discussion and coverage considered the tracing methods, topologies and control strategies in both industry and research fields. Commercial I–V tracers were reviewed in relation their sweep speeds, maximum ratings, resolutions, prices, data analysis abilities and sizes. This paper also made side-by-side comparisons using tables. Our summary provides an overview of the results, which can be used by designers to select the appropriate approach for I–V curve tracing. Based on the in-depth analysis, it can be concluded that the DC–DC converter method shows the advantage of flexibility and effectiveness to synthesise the merits of fast speed, high accuracy and ease of control. The DC–DC converter method is also considered a low-cost solution and demonstrates the potential to be further improved. The high-frequency switching operation causes ripples and increases the difficulty of smooth data acquisition. The dynamics of power converters also affect the operational speed for I–V curve tracing. These issues can be overcome by improving power conditioners and control strategies. For all the methods mentioned in this paper, the measurement points were unevenly distributed on the I–V curve. The issue should be resolved in the future to improve the acquisition accurracy and resolution.

Declaration of Competing Interest

The authors declare that they have no known competing financial interests or personal relationships that could have appeared to influence the work reported in this paper.

References

Aguilar, H.M., Maldonado, R.F., Navarro, L.B., 2017. Charging a capacitor with a photovoltaic module. Phys. Educ. 52, 045016.

Amiry, H., Benhmida, M., Bendaoud, R., Hajjaj, C., Bounouar, S., Yadir, S., Raïs, K., Sidki, M., 2018. Design and implementation of a photovoltaic iv curve tracer: Solar modules characterization under real operating conditions. Energy Convers. Manage. 169, 206–216.

Asghar, M.J., 2004. Power Electronics. PHI Learning Pvt Ltd.

Babaei, E., Mahmoodieh, M.E.S., 2014. Systematical method of designing the elements of the cuk converter. Int. J. Electrical Power Energy Syst. 55, 351–361.

Bai, J., Cao, Y., Hao, Y., Zhang, Z., Liu, S., Cao, F., 2015. Characteristic output of pv systems under partial shading or mismatch conditions. Sol. Energy 112, 41–54.

Balasubramanian, I.R., Ganesan, S.I., Chilakapati, N., 2013. Impact of partial shading on the output power of pv systems under partial shading conditions. IET Power Electron. 7, 657–666.

Batista, V.L.J., Chenlo, F., Afonso, J.L. 2012. Low-cost instrument for tracing current-voltage characteristics of photovoltaic modules. In: International Conference on Renewable Energies and Power Quality (ICREPQ'12).

Bifaretti, S., Iacovone, V., Cinà, L., Buffone, E., 2012. Global mppt method for partially shaded photovoltaic modules. In: 2012 IEEE Energy Conversion Congress and Exposition (ECCE). IEEE, pp. 4768–4775.

Chen, Z., Lin, W., Wu, L., Long, C., Lin, P., Cheng, S., 2018. A capacitor based fast iv characteristics tester for photovoltaic arrays. Energy Procedia 145, 381–387.

De Blas, M., Torres, J., Prieto, E., Garcıa, A., 2002. Selecting a suitable model for characterizing photovoltaic devices. Renewable Energy 25, 371–380.

Dhimish, M., Holmes, V., Mehrdadi, B., Dales, M., Chong, B., Zhang, L., 2017. Seven indicators variations for multiple pv array configurations under partial shading and faulty pv conditions. Renewable Energy 113, 438–460.

Dian, S., Wen, X., Deng, X., Zhang, S., 2014. Digital control of isolated cuk power factor correction converter under wide range of load variation. IET Power Electron. 8, 142–150.

DS-1000 (2016-01). DS-1000 I-V curve tracer user manual. Daystar.

Durán, E., Andújar, J., Enrique, J., Pérez-Oria, J. 2012. Determination of pv generator iv/pv characteristic curves using a dc-dc converter controlled by a virtual instrument. Int. J. Photoenergy, 2012.

Durán, E., Galán, M., Sidrach-de Cardona, A.J., 2009. Measuring the iv curve of photovoltaic generators-analyzing different dc–dc converter topologies. IEEE Ind. Eelectron. Mag. 4–14.

Duran, E., Piliougine, M., Sidrach-de Cardona, M., Galan, J., Andujar, J. 2008. Different methods to obtain the i–v curve of pv modules: a review. In: 2008 33rd IEEE Photovoltaic Specialists Conference. IEEE, pp. 1–6.

El Hammoumi, A., Motahhir, S., Chalh, A., El Ghzizal, A., Derouich, A., 2018. Low-cost virtual instrumentation of pv panel characteristics using excel and arduino in comparison with traditional instrumentation. Renewables: Wind Water Solar 5, 3.

Fernández-Reche, J., Cañadas, I., Sánchez, M., Ballestrín, J., Yebra, L., Monterreal, R., Rodríguez, J., García, G., Alonso, M., Chenlo, F., 2006. Psa solar furnace: a facility for testing pv cells under concentrated solar radiation. Solar Energy Mater. Solar Cells 90, 2480–2488.

Guvench, M., Gurcan, C., Durgin, K., MacDonald, D. 2004. Solar simulator and iv measurement system for large area solar cell testing. Age 9, 1.

Haque, A., Bharath, K.V.S., Khan, M.A., Khan, I., Jaffery, Z.A., 2018. Fault diagnosis of photovoltaic modules. Energy Sci. Eng.

Heckttheuer, L.A., Krenzinger, A., Prieb, C.W.M., 2002. Methodology for photovoltaic modules characterization and shading effects analysis. J. Braz. Soc. Mech. Sci. 24, 26–32.

Henni, O., Belarbi, M., Haddouche, K., Belarbi, E.-H., 2017. Design and implementation of a low-cost characterization system for photovoltaic solar panels. Int. J. Renewable Energy Res. (IJRER) 7, 1586–1594.

Hernday, P., 2014. Interpreting i–v curve deviations. Solar Professional 17–29.

Huang, P.-H., Xiao, W., Peng, J.C.-H., Kirtley, J.L., 2016. Comprehensive parameterization of solar cell: Improved accuracy with simulation efficiency. IEEE Trans. Industr. Electron. 63, 1549–1560.

I-V500w (2015–05-17). I-V curve tracer and IVCK tester up to 15A or 1500VDC. HT-Italia.

IEC 60891:2009, 2009. Procedures for temperature and irradiance corrections to measured I-V characteristics. Standard International Electrotechnical Commission Geneva, Switzerland.

IEC 60904-1:2006, 2006. Measurement of Photovoltaic Current-voltage Characteristic. Standard International Electrotechnical Commission Geneva, Switzerland.

IEC 62446-1. 2016. Photovoltaic (PV) Systems – Requirements For Testing, Documentation And Maintenance – Part 1: Grid Connected Systems – Documentation, Commissioning Tests And Inspection. Standard International Electrotechnical Commission Geneva, Switzerland.

IVT-200-1000. 2017–09. IVT-200-1000 data sheet. Kewell.

Kuai, Y., Yuvarajan, S., 2006. An electronic load for testing photovoltaic panels. J. Power Sources 154, 308–313.

Leite, V., Batista, J., Chenlo, F., Afonso, J.L. 2014. Low-cost iv tracer for photovoltaic modules and strings. In: 2014 International Symposium on Power Electronics, Electrical Drives, Automation and Motion. IEEE, pp. 971–976.

Leite, V., Chenlo, F. 2010. An improved electronic circuit for tracing the iv characteristics of photovoltaic modules and strings. In: Proceedings of the International Conference on Renewable Energies and Power Quality (ICREPQ'10). European Association for the Development of Renewable Energies, Environment and Power Quality.

Mahmoud, M.M., 2006. Transient analysis of a pv power generator charging a capacitor for measurement of the i–v characteristics. Renewable Energy 31, 2198–2206.

Mahmoud, Y.A., Xiao, W., Zeineldin, H.H., 2013. A parameterization approach for enhancing pv model accuracy. IEEE Trans. Industr. Electron. 60, 5708–5716.

Malik, A., Damit, S.J.B.H., 2003. Outdoor testing of single crystal silicon solar cells. Renewable Energy 28, 1433–1445.

MP-180. 2016. MP-180 I-V Tracer Technical Specifications. EKO.

Papageorgas, P., Piromalis, D., Valavanis, T., Kambasis, S., Iliopoulou, T., Vokas, G., 2015. A low-cost and fast pv iv curve tracer based on an open source platform with m2m communication capabilities for preventive monitoring. Energy Procedia 74, 423–438.

Piliougine, M., Carretero, J., Mora-López, L., Sidrach-de Cardona, M., 2011. Experimental system for current–voltage curve measurement of photovoltaic modules under outdoor conditions. Prog. Photovolt.: Res. Appl. 19, 591–602.

PV-8150K. 2013-01. PV-8150K I-V curve tracer. Qunling.

PV210. 2017–09-03. PV200/PV210 user manual. Seaward.

PVA-1000S. 2014-02. Solmetric PV Analyzer I-V Curve Tracer with SolSensor PVA-1000S, PVA-600. Solmetric.

PVPM1500X. 2018–06-01. PVPM1500X data sheet. PVE.

Recart, F., Mackel, H., Cuevas, A., Sinton, R. 2006a. Simple data acquisition of the current-voltage and illumination-voltage curves of solar cells1. In 2006 IEEE 4th World Conference on Photovoltaic Energy Conference (pp. 1215–1218). IEEE volume 1.

Recart, F., Mackel, H., Cuevas, A., Sinton, R. 2006b. Simple data acquisition of the current-voltage and illumination-voltage curves of solar cells1. In: 2006 IEEE 4th World Conference on Photovoltaic Energy Conference. IEEE vol. 1, pp. 1215–1218.

Riley, C.W. 2014. An autonomous online iv tracer for pv monitoring applications.

Rivai, A., Rahim, N.A., 2013. A low-cost photovoltaic (pv) array monitoring system. In: 2013 IEEE Conference on Clean Energy and Technology (CEAT). IEEE, pp. 169–174.

Rivai, A., Rahim, N.A., 2014. Binary-based tracer of photovoltaic array characteristics. IET Renew. Power Gener. 8, 621–628.

Sabudin, S.N.M., Jamil, N.M., Rosli, N., 2017. A review of parameter estimation used in solar photovoltaic system for a single diode model. J. Phys: Conf. Ser. 890, 012037.

Safari, A., Mekhilef, S., 2011. Simulation and hardware implementation of incremental conductance mppt with direct control method using cuk converter. IEEE Trans. Industr. Electron. 58, 1154–1161.

Sahbel, A., Hassan, N., Abdelhameed, M.M., Zekry, A., 2013. Experimental performance characterization of photovoltaic modules using daq. Energy Procedia 36, 323–332.

SOLAR-600, 2010. Amprobe SOLAR 600 Solar Analyzer Data Sheet. Amprobe.

Spertino, F., Ahmad, J., Ciocia, A., Di Leo, P., Murtaza, A.F., Chiaberge, M., 2015. Capacitor charging method for i–v curve tracer and mppt in photovoltaic systems. Sol. Energy 119, 461–473.

Spertino, F., Ahmad, J., Di Leo, P., Ciocia, A., 2016. A method for obtaining the iv curve of photovoltaic arrays from module voltages and its applications for mpp tracking. Sol. Energy 139, 489–505.

Spertino, F., Sumaili, J., Andrei, H., Chicco, G., 2013. Pv module parameter characterization from the transient charge of an external capacitor. IEEE J. Photovolt. 3, 1325–1333.

Spiliotis, K., Yordanov, G., Van den Broeck, G., Goverde, H., Baert, K., Driesen, J. 2017. Towards accurate, high-frequency iv curve measurements of photovoltaic modules applying electronic loads. In: 33rd European Photovoltaic Solar Energy Conference and Exhibition. WIP; Sylvensteinstrasse 2, D-81369 Munich, Germany, pp. 1561–1565.

Triki-Lahiani, A., Abdelghani, A.B.-B., Slama-Belkhodja, I., 2018. Fault detection and

monitoring systems for photovoltaic installations: a review. Renew. Sustain. Energy Rev. 82, 2680–2692.
Tse, K., Ho, B.M., Chung, H.-H., Hui, S.R., 2004. A comparative study of maximum-power-point trackers for photovoltaic panels using switching-frequency modulation scheme. IEEE Trans. Industr. Electron. 51, 410–418.
Van Dyk, E., Gxasheka, A., Meyer, E., 2005. Monitoring current–voltage characteristics and energy output of silicon photovoltaic modules. Renewable Energy 30, 399–411.
Willoughby, A.A., Osinowo, M.O., 2018. Development of an electronic load iv curve tracer to investigate the impact of harmattan aerosol loading on pv module pern2tkformance in southwest nigeria. Sol. Energy 166, 171–180.
Xiao, W., 2017. Photovoltaic Power System: Modeling, Design and Control. Wiley.
Xiao, W., Dunford, W.G., Palmer, P.R., Capel, A., 2007. Regulation of photovoltaic voltage. IEEE Trans. Industr. Electron. 54, 1365–1374.
Xiao, W., Ozog, N., Dunford, W.G., 2007. Topology study of photovoltaic interface for maximum power point tracking. IEEE Trans. Industr. Electron. 54, 1696–1704.
Xiong, Q., Ji, S., Liu, X., Feng, X., Zhang, F., Zhu, L., Gattozzi, A.L., Hebner, R.E., 2018. Detecting and localizing series arc fault in photovoltaic systems based on time and frequency characteristics of capacitor current. Sol. Energy 170, 788–799.
Zhu, Y., 2018. An adaptive IV curve detecting method for photovoltaic modules. In: 2018 IEEE International Power Electronics and Application Conference and Exposition (PEAC). IEEE, pp. 1–6.